3D kinetic Monte-Carlo simulations of diamond growth on (1 0 0) surfaces

Audrey Valentin, Ovidiu Brinza, Samir Farhat, Jocelyn Achard, Fabien Bénédic

3D kinetic Monte-Carlo simulation of diamond growth on (1 0 0) surfaces

Audrey Valentin, Ovidiu Brinza, Samir Farhat, Jocelyn Achard and Fabien Bénédic*

Université Sorbonne Paris Nord, LSPM, CNRS, UPR3407, F-93430 Villetaneuse, France
E-mail: audrey.valentin@lspm.cnrs.fr

Keywords : kinetic Monte-Carlo simulation, single-crystal diamond, diamond growth

Abstract

A 3D Kinetic Monte-Carlo (KMC) model is implemented and used to simulate the growth of (1 0 0)-oriented diamond layers. The model considers four processes: adsorption and desorption of CH_3 radicals, etching of carbon atoms and migration of adsorbed carbon-containing species. The atomic structure of diamond is taken into account including the formation of dimer rows on the surface. The model correctly reproduces the step-flow growth mechanism of diamond (1 0 0) surfaces and the obtained growth rates are close to experimental data. The propagation of the steps show a clear anisotropy. Steps are usually two atomic layers high but step bunching can be observed in presence of defects. The model thus can be used as a predictive tool to obtain growth rates and to understand the effect of atomic effects on the layer morphology.

1. Introduction

Plasma-assisted growth of diamond layers with a very low concentration of defects is a key issue to improve the performance of diamond-based electronic devices. For example, it has been shown that the electrical performance of Schottky diodes is highly correlated to the crystalline quality of the active diamond layer [1]. The same conclusion can also be drawn about particle detectors [2].

By contrast, a higher density of impurities and vacancies is needed to improve quantum devices. This includes N-V center-based devices, which are fabricated on diamond layers containing controlled levels of nitrogen introduced either by doping during the growth [3] or by nitrogen implantation [4]. Quantum grade material can be also improved using processes such as He ion implantation [5] or electron irradiation [6] to increase the number of vacancies.

In all cases, the optimization of the diamond growth processes requires a detailed knowledge of the mechanisms involved. To that aim, a simulation tool that connects the experimental conditions (with a detailed knowledge of the plasma content and state) to the final crystal morphology must be developed. Such a simulation tool has several components: (i) the plasma composition and state have to be determined as a function of process parameters (the reactor geometry, the feed gas composition and pressure, the power…), (ii) then the growth process has to be studied to find how the plasma components interact with the substrate surface to build a diamond layer, and (iii) finally the obtained growth rates have to be used to define the final crystal morphology. While component (i) deals with various species (atoms, molecules, radicals…) and chemical reactions, component (iii) is a macroscopic geometrical model. Component (ii) has to link both scales to build a multi-scale modelling tool.

Simulators (i) and (iii) in such a tool are already available. The composition of the plasma involved in the growth process has been obtained with a model working in H_2/CH_4 gas mixture that has been developed for several years [7]. Furthermore, the final crystal geometry is easily calculated from the growth rates with a geometric model [8]. However, this

model does not take the defects into account. The aim of this study is therefore to focus on component (ii), to get the growth rates from the plasma composition and to study the appearance of defects in the layers.

Such a simulation can be performed with ab initio, Kinetic Monte-Carlo (KMC), or continuum models [9]. Ab initio simulations are limited to a few tens of atoms, which is not sufficient to observe the appearance and the development of extended defects. Continuum models, on the contrary, can be used to model thick and large layers, but do not provide a clear view of the microscopic mechanisms responsible for the appearance of point defects such as vacancies or impurities. Between both approaches, KMC modelling constitutes a good compromise. Such models show the step flow process responsible for the crystal growth of a several tens of atomic layers, with a reasonable computation time.

This paper thus focuses on the development of a KM model and on the results obtained, which is to be part of the multi-scale modelling of diamond growth. KMC models rely on a set of processes the probabilities of which are known: at each time step, a process is randomly selected. Building a KMC thus requires selecting the processes to include in the model and to find their rates. In the first part, after having summed up the results obtained by other authors, we will present the main characteristics of our KMC model. Then, in the second part, the results will be presented, and compared to experimental results obtained in previous works.

2. The model

2.1. Kinetic Monte-Carlo modelling

Several teams have used KMC simulations to model diamond growth. Pioneering works focused on growth of (1 0 0) [10] and (1 1 1) surfaces [11] with 3D models taking into account adsorption and desorption of many chemical species. The chemical rates taken into account in the models were calculated or extracted from experimental data. Grujicic et al. [12] used a detailed set of 68 surface-reaction kinetics of (111)- and ((100)-oriented diamond associated with CVD reactions which rates were calculated with the ChemKin software [13]. Their KMC simulator was coupled to a plasma simulation, to obtain a multi-scale model with a good predicting power regarding the effects of the substrate temperature and the mole fraction of CH_4 in the feed gas on the deposition rates of (111- and (100)-oriented diamond films. However, the migration of the radicals at the surface was not taken into account. This issue was addressed in a publication by Netto et al. [14] where the combination between adsorption, desorption and migration was investigated. The calculated growth rates showed a reasonable agreement with experimental results but the film morphology was not accurately reproduced.

All those works used an accurate description of the crystal lattice. A lighter framework was introduced by May *et al*., [15] with a crystal lattice simplified to aligned square blocks in two dimensions, and a growth description limited to 3 possible processes: adsorption, desorption and migration. The rates were obtained with a chemical model previously developed by the same team [16] and the KMC simulation results were in good agreement with those obtained with this model. The crystalline nature of the obtained layer (nanocrystalline, polycrystalline or monocrystalline) was related to the surface roughness, without considering grain boundaries nor grain orientation. The nucleation process was considered as the meeting of two adsorbed, migrating radicals. The radicals then stop migrating and they are considered as inserted into the crystal lattice. The set of processes was later completed with adsorption

of various species, direct insertion of atoms in the lattice and etching [17]. The lattice was also represented in 3D, but still with aligned blocks [18]. This model thus uses a carefully selected set of chemical processes but still lacks a relevant description of the crystal lattice, which prevents defects to be correctly taken into account.

2.2. The KMC simulator

The KMC simulator was implemented using Processing [19] which is a free, open source software.

We performed 3D simulations fully taking into account the crystal geometry. The surface is a (1 0 0) plane on which the growth process occurs. Periodic boundary conditions are applied to avoid boundary effects: atoms on one side are considered to be bounded to the atoms at the other side. Carbon-containing chemical species formed in the plasma are adsorbed on the diamond surface to form surface radicals, which can migrate on the surface. The surface reconstruction is not taken into account but two adjacent surface radicals can form a dimer. The formation of dimer rows has indeed been identified as an important aspect of (1 0 0) surface growth[20]. Once the carbon species is involved in a dimer bond, it is considered as inserted into the diamond lattice.

The simulations follow a classical KMC algorithm [21]. Before each event, the list of all the processes that can occur at each site is constituted. The time τ between two events is then randomly selected following the formula:

$$\tau = -\log\frac{U}{\Gamma_{Tot}} \quad (1)$$

where *U* is a random number selected between 0 and 1, and Γ_{Tot} is the sum of all process rates. Then another random number is used to select one process between all possible processes according to their respective rates (that procedure in well explained in [11]).

The simulation stops when a layer is completed. The final time *t* is the sum of all the times τ between two events and gives the growth rate G:

$$G = \frac{a}{4t} \quad (2)$$

where *a* = 3.57 Å is the diamond lattice parameter.

The set of processes was selected to reproduce the model proposed by Harris and Goodwin [22]. Four processes are thus taken into account as illustrated on Figure 1:

- Adsorption of a radical on the diamond surface,
- Desorption of an adsorbed radical,
- Etching of a lattice atom,
- Surface migration of an adsorbed radical.

The processes of activation and deactivation of surface sites are not taken into account in the KMC code, contrary to some other works [12,14,15]. In our case, the ratio of active sites R_H, which has been given in [16], is taken into account in the adsorption rate.

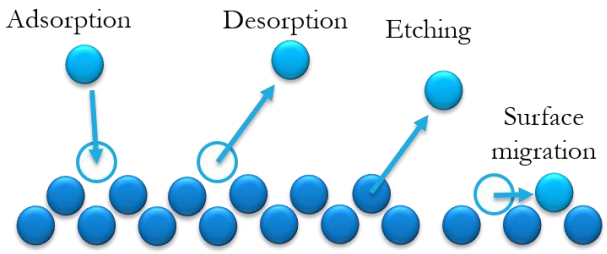

Figure 1. Processes taken into account in the model.

When a radical is adsorbed on the surface, it can desorb or migrate. The migrating radical can move along or across the dimer line, or go down a step edge. It has indeed been demonstrated that all these processes have the same probability [14]. Inserted atoms can only be etched (Figure 2a). Each carbon species is considered as adsorbed until it finds another carbon with which a dimer can be formed. Both carbons are then considered as inserted into the lattice (Figure 2b). A new dimer row can be created when two radicals meet along a step edge. The formation of a new dimer row is not allowed far from a step edge: this germination process follows mechanisms that are not yet taken into account in the model. For this reason, all simulations are performed with an initial germ.

According to previous authors [14], the 2 carbon dimer constitutes the critical nucleus for diamond growth so that its formation rate is much higher than all the other processes taken into account in our model. We thus considered that dimer formation is immediate.

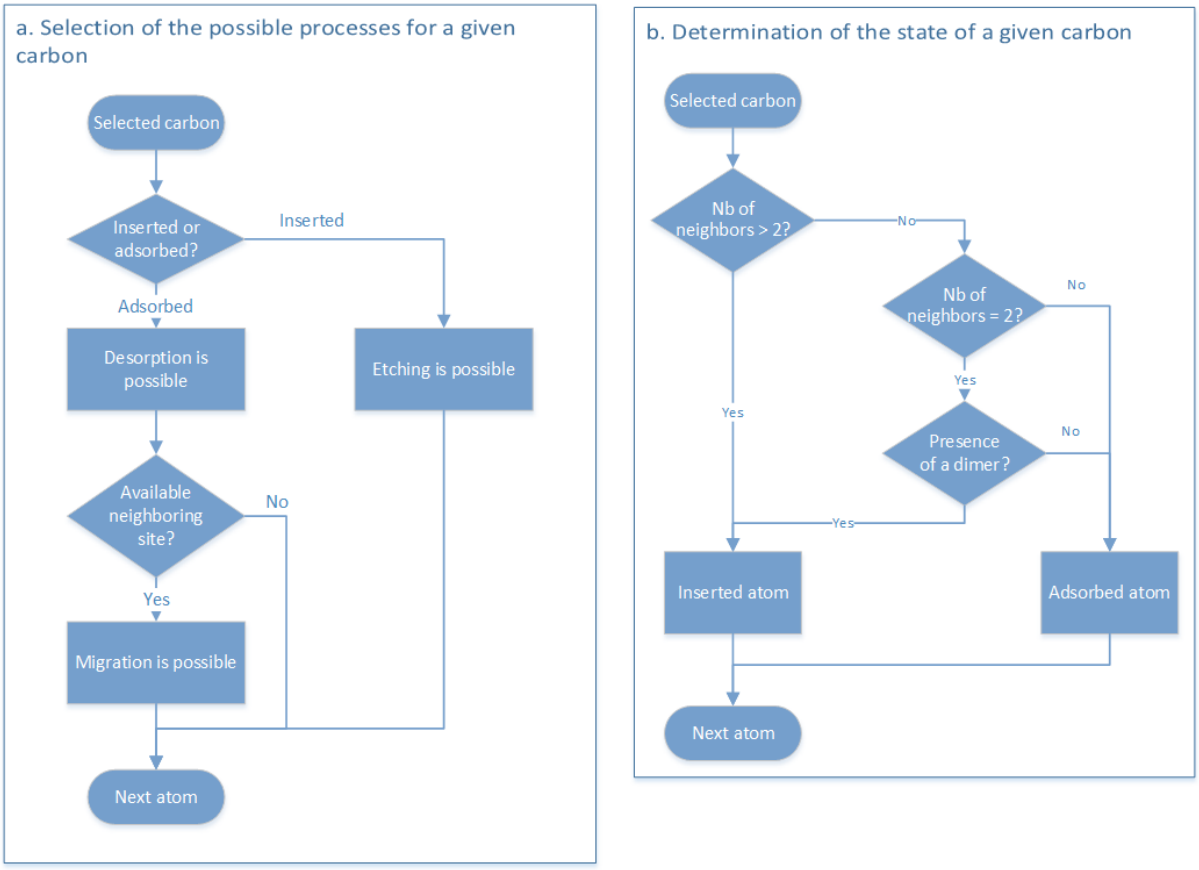

Figure 2. Determination of the possible processes (a) and of the state (adsorbed radical or inserted atom) of a given carbon atom (b).

2.3. Process rates

The four process rates have already been established by several teams and are given in Table 1. In this model, we only consider the adsorption of CH_3, following the growth mechanisms suggested by Harris and Goodwin.

The sticking coefficient *S* has been set to various values in previous works [15,17]. However, it has been shown that the sticking coefficient varies with the substrate temperature [23]. The sticking coefficient has thus been fitted to reproduce the experimental growth rates. This parameter is the only one that is fitted in this model.

Process	Frequency	Terms	Sources
Adsorption	$\sqrt{\frac{8k_BT}{\pi \times M_{CH_3}}}\frac{[CH_3]}{4} \times \rho \times S \times R_H$	M_{CH_3} : mass of a methyl radical ρ : diamond surface density S: sticking coefficient (see text for details) R_H : ratio of active sites	[15,16]
Desorption	$\frac{k_BT}{\mathrm{h}} exp\left(-\frac{G_d}{RT}\right)$	$G_d = 200kJ/mol$: Gibbs energy of activation	[18]
Etching	$\frac{k_BT}{\mathrm{h}} exp\left(-\frac{G_d}{RT}\right) exp\left(-\frac{\varepsilon N_N G_d}{RT}\right)$	$\varepsilon = 0.365$: etching factor N_N: number of bonds	
Surface migration	$6.13 \times 10^{13} \times exp\left(-\frac{18269}{T}\right) \times R_H$	R_H: ratio of active sites	[14]

Table 1. Process rates used in the model. k_B is the Boltzmann constant, *h* is the Planck constant, R is the universal gas constant and T is the substrate temperature.

The substrate temperature *T*, the surface methyl radical concentration $[CH_3]$, and the surface atomic hydrogen concentration [*H*] that is used to calculate R_H were taken from a previous study [24].

The resulting rates are given in Figure 3. The migration rate is predominant at all temperatures and etching is low. At low temperature, desorption is lower than adsorption when at higher temperatures, desorption tends to be much more important than adsorption.

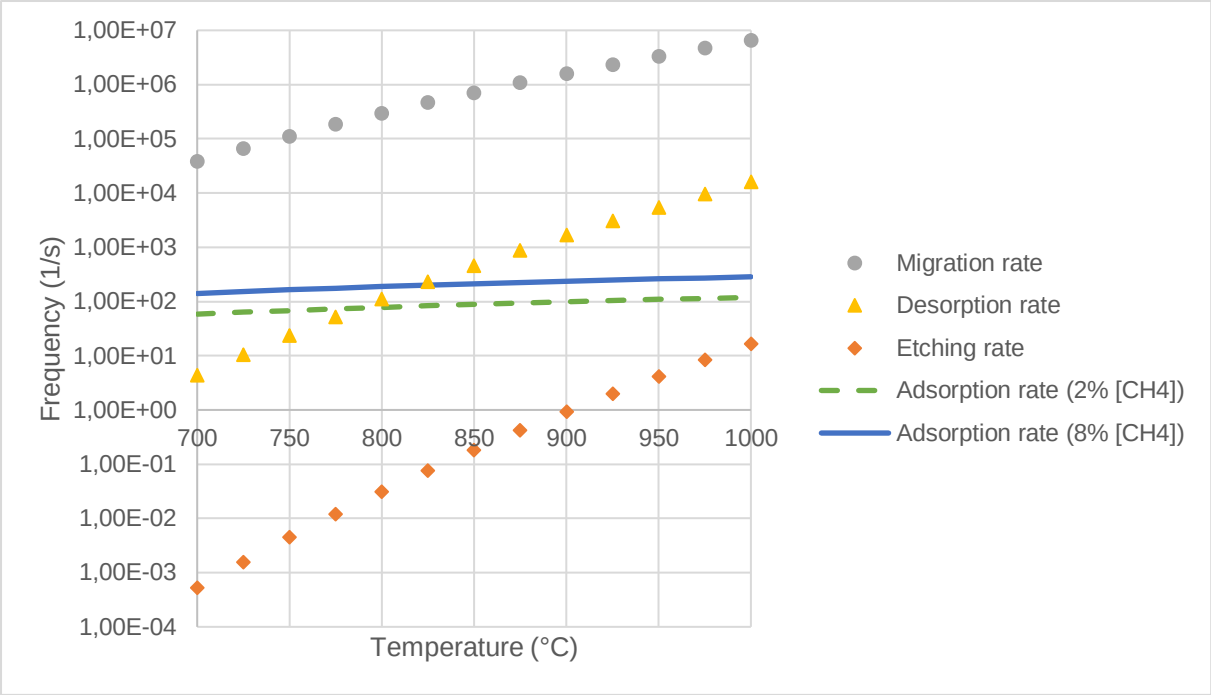

Figure 3. Process rates vs the substrate temperature.

3. Results

3.1. Growth rates

The calculated growth rates are compared to the experimental growth rates [25] on Figure 4. The fitting of the sticking coefficient leads to a good reproduction of the temperature dependence of the growth rates. We have observed that the obtained values follow an Arrhenius law,

$$S = S_0 exp\left(-\frac{E_a}{RT}\right) \quad (3)$$

where $S_0 = 85$, $E_a = 50\ kJ/mol$. With this expression, the sticking coefficient becomes high at high temperature (0.75 at 950°C), with values higher than the ones provided by other teams [15,17,23]. However, in that case, germination of new aggregates gets more likely. This process is not taken into account in this model. The high value of the sticking coefficient is then supposed to compensate for the absence of germination.

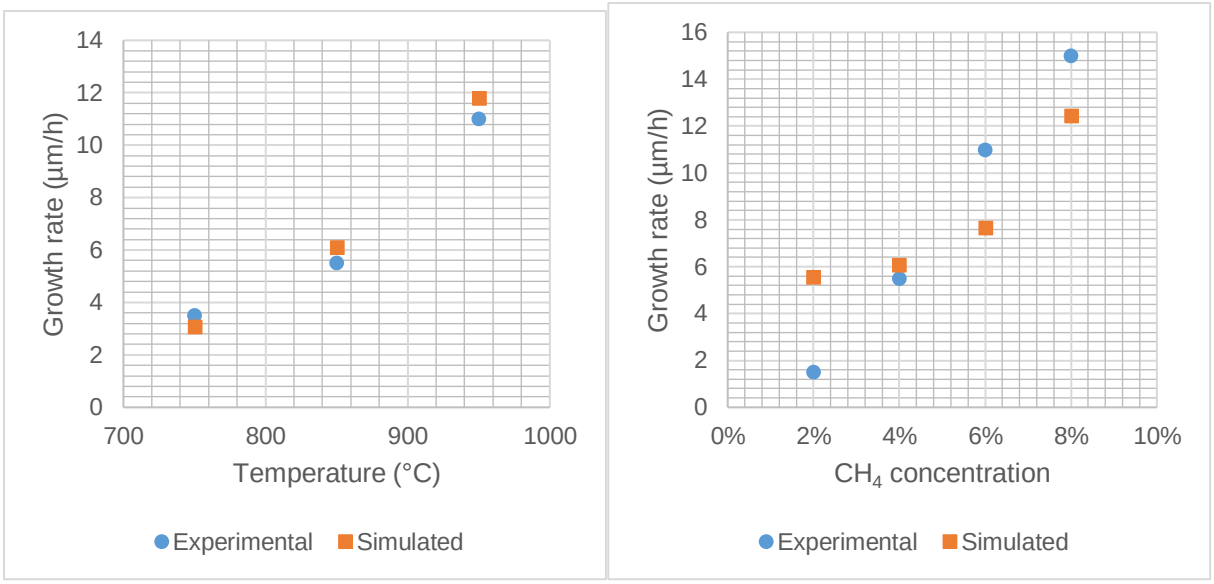

Figure 4. Calculated and experimental growth rates. On the left, growth rates are obtained at various temperatures and a 4% methane concentration in the gas phase. On the right, growth rates are obtained at various methane concentrations at 850°C. The couple pressure/microwave power is 200 mbar/3 kW in both cases.

The growth rate dependence on the methane concentration shows a light discrepancy between simulation and experimental results, which can be attributed to the use of the Harris and Goodwin model. This model indeed gives a simplified view of the chemical processes involved. The trend is however reproduced, with a growth rate that increases with the methane concentration and the correct order of magnitude.

3.2. Growth of a single layer

The growth of a single diamond layer on an already complete layer is presented at different times on Figure 5. All images are a top view of the diamond surface, with the dimer rows oriented horizontally. The crystal grows in two directions, horizontally and vertically. Adsorbed radicals appear in blue while inserted atoms appear in gray. A video of the corresponding simulation is given in supplementary material.

In this simulation, an initial germ is constituted of three dimer rows with four atoms each (a). The germ first expands in the dimer row direction (b). Then, new dimer rows are formed and the germ expands (c to e) until the whole surface is covered (f). The germ is limited by four step edges, with two step edges aligned on the dimer rows and the two others perpendicular to the dimer rows, which move on the diamond surface. We then reproduce the well-known step flow growth process. As expected, the step edges progress more slowly when they are parallel to the dimer rows (horizontal edges) than when they are perpendicular to them (vertical edges). In the latter case, the adsorbed and migrating radicals can stick to any point of the step edge, whereas in the former case, only two positions allow the formation of a dimer allowing the step to progress. For the same reason, vertical step edges have an indented profile whereas the horizontal ones are straighter. All these observations are consistent with STM images of diamond surfaces [26].

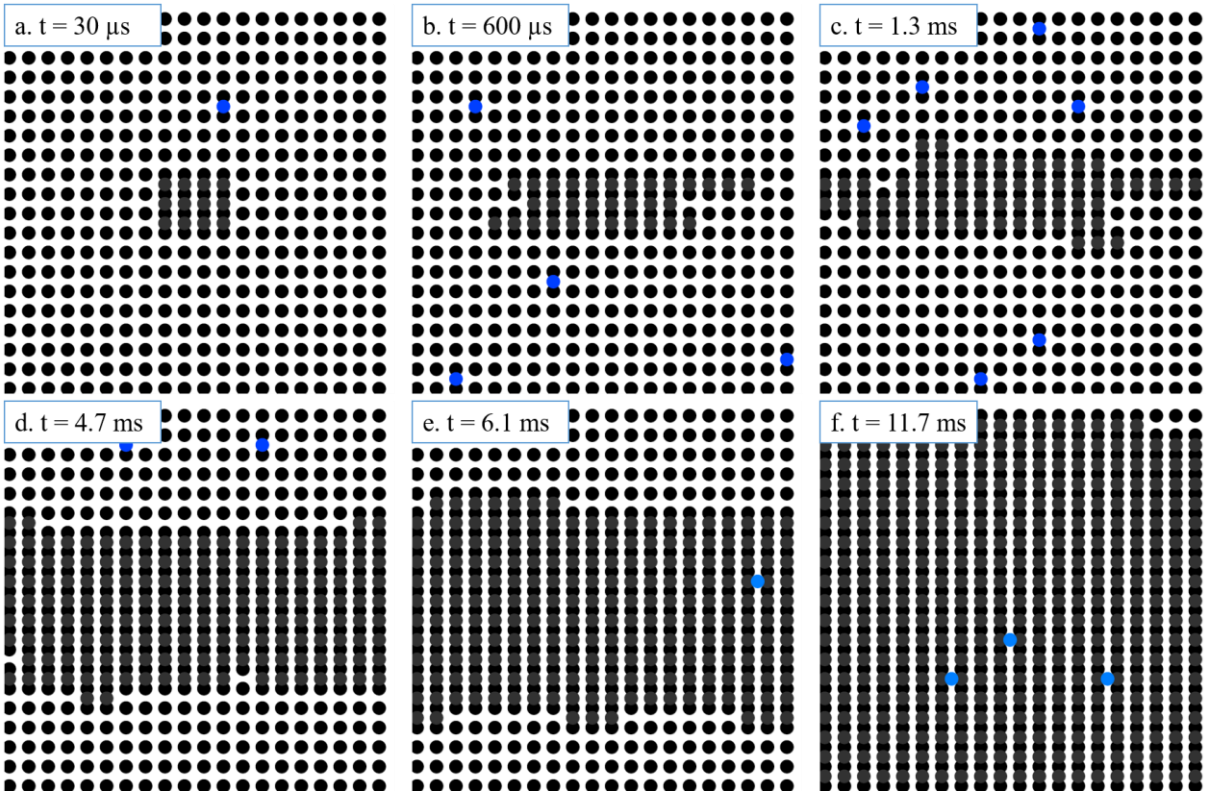

Figure 5. Growth of a single diamond layer (top view), for a temperature of 850°C, 4% methane concentration in the gas phase and a couple pressure/microwave power set to 200 mbar/3 kW.

The evolution of the germ at various temperatures is shown on Figure 6. At low temperature (a), the germ expands in both directions: with a lower desorption, many adsorbed radicals are available to form new dimer rows. At medium and high temperatures (b and c), the layer is shaped like a ribbon expanding in the dimer row direction. In these cases, the desorption process is more important and decreases the number of adsorbed radicals, decreasing the probability of formation of a new dimer row. The horizontal step edges are even straighter at higher temperature (c) than at medium temperature (b).

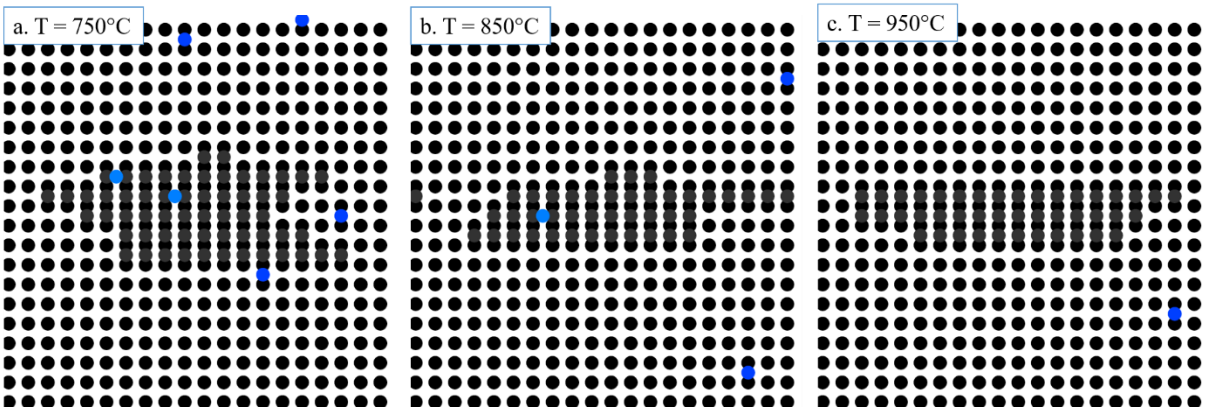

Figure 6. Growth of a single diamond layer (top view), for different temperatures, with 4% methane concentration in the gas phase and a couple pressure/microwave power set to 200 mbar/3 kW.

3.3. Vicinal surface

To simulate diamond growth on a vicinal surface, the initial germ was replaced with three steps which position was set to reproduce a 5° misorientation. This angle was chosen to keep a relatively low number of atomic sites in the model: with a higher angle, the number of layers has to be increased while with a lower angle, the number of atomic sites per layer has to be included. The step center is located at the middle of the simulation window to ensure a correct use of periodic boundary conditions.

The results are shown on Figure 7. Figure 7a presents the initial configuration, while Figure 7b and Figure 7c show the evolution of the steps. The corresponding video is given in supplementary material.

The bottom step grows along the dimer rows. It is then a fast step, which is rapidly completed. Above this first step, the second one grows slowly across the dimer rows. The top step is, again, a fast one growing along the dimer rows. The growth process begins with the fast steps (bottom and top) which rapidly occupy all the available space (Figure 7b). The top step can only cover the terrace limited by the slow step. The growth process is then driven by the progression of this slow step (Figure 7c).

We then obtained a step flow growth process, with two atomic layers high steps (Figure 8). This reproduces experimental observations [26,27].

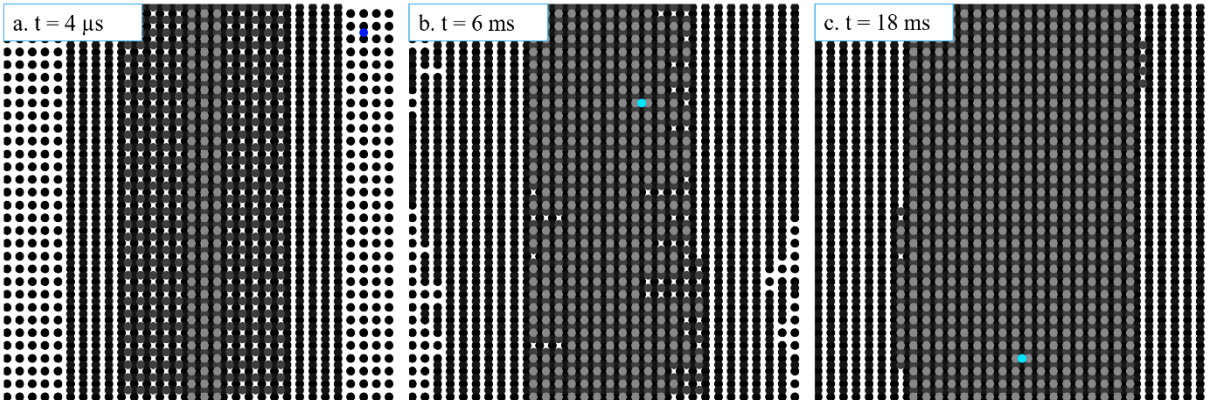

Figure 7. Growth of three diamond layers (top view) on a vicinal surface, for a temperature of 850°C, with 4% methane concentration in the gas phase and a couple pressure/microwave power set to 200 mbar/3 kW.

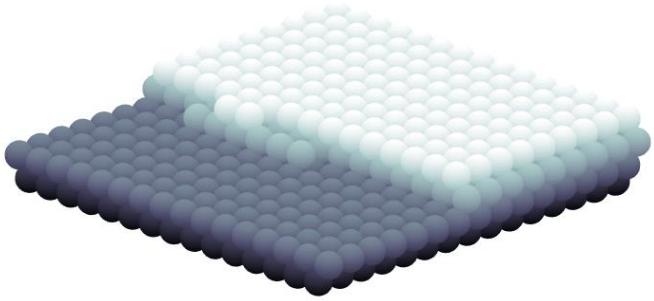

Figure 8. 3D view of a detail of the step edge (same conditions as Figure 7).

3.4. Step bunching

We finally performed a simulation with 6 atomic layers. Vacancies were included in the first and second layers, simply by forbidding any radical to be attached to this particular atomic site. These vacancies appear in green on Figure 9.

At the beginning of the simulation, the 5 step edges are close to each other, next to the middle of the simulation window (Figure 9a). Then, the fast step edges join the slow step edges, to constitute the two layers steps that we already obtained in the previous simulations (Figure 9b). The vacancies are embedded in the second layer, because of the rapid progress of the step edge. The completion of this layer is due to the periodic boundary conditions: the atoms inserted in the lattice around the vacancy are linked to the dimer rows originating from the closest step on one side and from the symmetric step through the periodic boundary conditions on the other side. The slow steps are slowed down by the vacancies: the radicals migrating on top of the vacancy are bonded only to one lattice atom, which increase their desorption probability. They are finally caught up by the top layers (Figure 9c). This causes a step bunching with four atomic steps, as displayed on Figure 10. This step bunching occurs if the vacancy is included in a fast step as well as in a slow step.

Step bunching is experimentally observed in the presence of impurities, especially nitrogen [3,28]. The defect modelled here is however a vacancy. We still need to clarify why the morphology experimentally attributed to impurities appears here in presence of vacancies. We assume that these vacancies are associated to impurities: in that case, the step bunching is not simply due to the presence of nitrogen, but of NV centers.

Besides, the rounded shape of the macrosteps calculated in [28] does not appear here. This shape is attributed to the step line tension, which is not taken into account by the model. Our KMC simulation can thus explain why step bunching occurs but not reproduce precisely the macro step shape. This result is, however, a progress in our understanding of diamond growth processes.

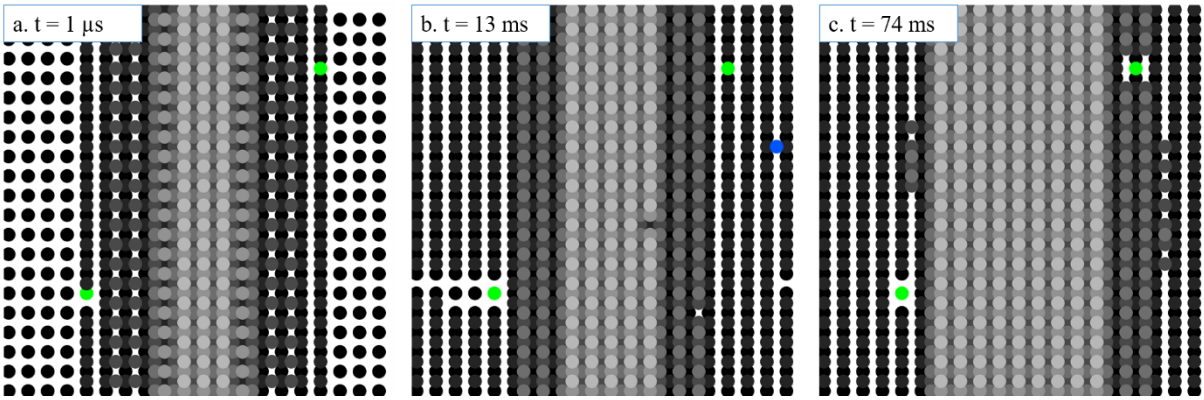

Figure 9. Growth of three diamond layers (top view) on a (1 0 0) surface with a vacancy embedded in the lowest layer, for a temperature of 850°C, with 4% methane concentration in the gas phase and a couple pressure/microwave power set to 200 mbar/3 kW.

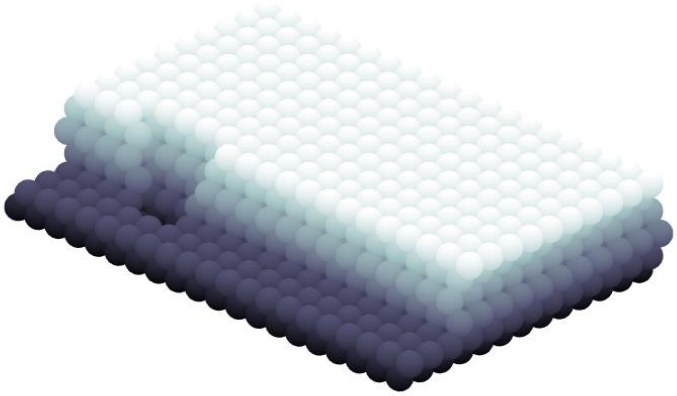

Figure 10. 3D view of a detail of the step edge (same conditions as Figure 9).

4. Conclusion

A 3D kinetic Monte-Carlo model was used to simulate microwave plasma -assisted diamond growth in the (1 0 0) direction. Our model considers adsorption, desorption, etching and surface migration. We used accurate values for gas and surface concentrations for process conditions available from our models and experiments. The model parameters were fitted to reproduce the experimental growth rates. We performed a large number of simulations covering a wide range of deposition conditions. Simulations correctly reproduces the step flow growth process thereby underlying major chemical kinetics of the CVD system and a difference in the step velocity related to its orientation is shown. The importance of correctly taking into account the surface dimer rows has been highlighted. In accordance with experimental observations, the steps are two layers high. Growth of defective layers including vacancies induce step-bunching features, but the experimental curved shape of these steps is not restituted. New effects, such as germination, need to be taken into account in the model to improve the description of diamond growth. This model is however useful for predictive simulations and to explain the diamond layer morphology arising from atomic-scale phenomena.

Acknowledgements

This work has received funding from the European Union's research and innovation program through the ASTERIQS project under grant agreement n°820394 and from Université Sorbonne Paris Nord (BQR project).

References

[1] H. Umezawa, N. Tatsumi, Y. Kato, S. Shikata, Leakage current analysis of diamond Schottky barrier diodes by defect imaging, Diamond and Related Materials. 40 (2013) 56–59. https://doi.org/10.1016/j.diamond.2013.09.011.

[2] P. Bergonzo, D. Tromson, C. Descamps, H. Hamrita, C. Mer, N. Tranchant, M. Nesladek, Improving diamond detectors: A device case, Diamond and Related Materials. 16 (2007) 1038–1043. https://doi.org/10.1016/j.diamond.2006.11.099.

[3] A. Tallaire, A.T. Collins, D. Charles, J. Achard, R. Sussmann, A. Gicquel, M.E. Newton, A.M. Edmonds, R.J. Cruddace, Characterisation of high-quality thick single-crystal diamond grown by CVD with a low nitrogen addition, Diamond and Related Materials. 15 (2006) 1700–1707. https://doi.org/10.1016/j.diamond.2006.02.005.

[4] S. Pezzagna, B. Naydenov, F. Jelezko, J. Wrachtrup, J. Meijer, Creation efficiency of nitrogen-vacancy centres in diamond, New J. Phys. 12 (2010) 065017. https://doi.org/10.1088/1367-2630/12/6/065017.
[5] F. Fávaro de Oliveira, S.A. Momenzadeh, D. Antonov, J. Scharpf, C. Osterkamp, B. Naydenov, F. Jelezko, A. Denisenko, J. Wrachtrup, Toward Optimized Surface δ-Profiles of Nitrogen-Vacancy Centers Activated by Helium Irradiation in Diamond, Nano Lett. 16 (2016) 2228–2233. https://doi.org/10.1021/acs.nanolett.5b04511.
[6] C.A. McLellan, B.A. Myers, S. Kraemer, K. Ohno, D.D. Awschalom, A.C. Bleszynski Jayich, Patterned Formation of Highly Coherent Nitrogen-Vacancy Centers Using a Focused Electron Irradiation Technique, Nano Lett. 16 (2016) 2450–2454. https://doi.org/10.1021/acs.nanolett.5b05304.
[7] G. Lombardi, K. Hassouni, G.-D. Stancu, L. Mechold, J. Röpcke, A. Gicquel, Modeling of microwave discharges of H2 admixed with CH4 for diamond deposition, Journal of Applied Physics. 98 (2005) 053303. https://doi.org/10.1063/1.2034646.
[8] F. Silva, J. Achard, X. Bonnin, A. Michau, A. Tallaire, O. Brinza, A. Gicquel, 3D crystal growth model for understanding the role of plasma pre-treatment on CVD diamond crystal shape, Physica Status Solidi (a). 203 (2006) 3049–3055. https://doi.org/10.1002/pssa.200671101.
[9] A.C. Levi, M. Kotrla, Theory and simulation of crystal growth, J. Phys.: Condens. Matter. 9 (1997) 299–344. https://doi.org/10.1088/0953-8984/9/2/001.
[10] E.J. Dawnkaski, D. Srivastava, B.J. Garrison, Growth of diamond films on a diamond {001}(2×1):H surface by time dependent Monte Carlo simulations, J. Chem. Phys. 104 (1996) 5997–6008. https://doi.org/10.1063/1.471331.
[11] C.C. Battaile, D.J. Srolovitz, J.E. Butler, A kinetic Monte Carlo method for the atomic-scale simulation of chemical vapor deposition: Application to diamond, Journal of Applied Physics. 82 (1997) 6293–6300. https://doi.org/10.1063/1.366532.
[12] M. Grujicic, S.G. Lai, Multi-length scale modeling of CVD of diamond Part I A combined reactor-scale/atomic-scale analysis, Journal of Materials Science. 35 (2000) 5359–5369. https://doi.org/10.1023/A:1004851029978.
[13] R.J. Kee, F.M. Rupley, J.A. Miller, The Chemkin Thermodynamic Data Base, Sandia National Lab. (SNL-CA), Livermore, CA (United States), 1990. https://doi.org/10.2172/7073290.
[14] A. Netto, M. Frenklach, Kinetic Monte Carlo simulations of CVD diamond growth—Interlay among growth, etching, and migration, Diamond and Related Materials. 14 (2005) 1630–1646. https://doi.org/10.1016/j.diamond.2005.05.009.
[15] P.W. May, N.L. Allan, M.N.R. Ashfold, J.C. Richley, Y.A. Mankelevich, Simplified Monte Carlo simulations of chemical vapour deposition diamond growth, J. Phys.: Condens. Matter. 21 (2009) 364203. https://doi.org/10.1088/0953-8984/21/36/364203.
[16] P.W. May, Y.A. Mankelevich, From Ultrananocrystalline Diamond to Single Crystal Diamond Growth in Hot Filament and Microwave Plasma-Enhanced CVD Reactors: a Unified Model for Growth Rates and Grain Sizes, J. Phys. Chem. C. 112 (2008) 12432–12441. https://doi.org/10.1021/jp803735a.
[17] P.W. May, J.N. Harvey, N.L. Allan, J.C. Richley, Yu.A. Mankelevich, Simulations of chemical vapor deposition diamond film growth using a kinetic Monte Carlo model, Journal of Applied Physics. 108 (2010) 014905. https://doi.org/10.1063/1.3437647.
[18] W.J. Rodgers, P.W. May, N.L. Allan, J.N. Harvey, Three-dimensional kinetic Monte Carlo simulations of diamond chemical vapor deposition, J. Chem. Phys. 142 (2015) 214707. https://doi.org/10.1063/1.4921540.
[19] Processing official website, Processing. (n.d.). https://processing.org// (accessed October 14, 2021).
[20] T. Tsuno, T. Imai, Y. Nishibayashi, K. Hamada, N.F.N. Fujimori, Epitaxially Grown Diamond (001) 2×1/1×2 Surface Investigated by Scanning Tunneling Microscopy in Air, Jpn. J. Appl. Phys. 30 (1991) 1063. https://doi.org/10.1143/JJAP.30.1063.

[21] T.P. Schulze, Efficient kinetic Monte Carlo simulation, Journal of Computational Physics. 227 (2008) 2455–2462. https://doi.org/10.1016/j.jcp.2007.10.021.
[22] D.G. Goodwin, Scaling laws for diamond chemical-vapor deposition. I. Diamond surface chemistry, Journal of Applied Physics. 74 (1993) 6888–6894. https://doi.org/10.1063/1.355063.
[23] L. Schwaederlé, P. Brault, C. Rond, A. Gicquel, Molecular Dynamics Calculations of CH3 Sticking Coefficient onto Diamond Surfaces, Plasma Processes and Polymers. 12 (2015) 764–770. https://doi.org/10.1002/ppap.201400223.
[24] F. Silva, J. Achard, O. Brinza, X. Bonnin, K. Hassouni, A. Anthonis, K. De Corte, J. Barjon, High quality, large surface area, homoepitaxial MPACVD diamond growth, Diamond and Related Materials. 18 (2009) 683–697. https://doi.org/10.1016/j.diamond.2009.01.038.
[25] O. Brinza, J. Achard, F. Silva, X. Bonnin, P. Barroy, K.D. Corte, A. Gicquel, Dependence of CVD diamond growth rate on substrate orientation as a function of process parameters in the high microwave power density regime, Physica Status Solidi (a). 205 (2008) 2114–2120. https://doi.org/10.1002/pssa.200879716.
[26] Y. Kuang, Y. Wang, N. Lee, A. Badzian, T. Badzian, T.T. Tsong, Surface structure of homoepitaxial diamond (001) films, a scanning tunneling microscopy study, Appl. Phys. Lett. 67 (1995) 3721–3723. https://doi.org/10.1063/1.115361.
[27] W.J.P. van Enckevort, G. Janssen, W. Vollenberg, J.J. Schermer, L.J. Giling, M. Seal, CVD diamond growth mechanisms as identified by surface topography, Diamond and Related Materials. 2 (1993) 997–1003. https://doi.org/10.1016/0925-9635(93)90264-3.
[28] F.K. de Theije, J.J. Schermer, W.J.P. van Enckevort, Effects of nitrogen impurities on the CVD growth of diamond: step bunching in theory and experiment, Diamond and Related Materials. 9 (2000) 1439–1449. https://doi.org/10.1016/S0925-9635(00)00261-2.